On Some New Results of Broadband Meter/ Decimeter Observations

Henry Aurass
Astrophysikalisches Institut Potsdam, Solare Radioastronomie, An der Sternwarte 16, Potsdam, D–14482, Germany
E-mail: aurass@iap.de

Abstract

With special emphasis on the radio signature of coronal shock waves (type II bursts) we review radio spectral observations in the decimeter to meter wave range. In a second part, we demonstrate that a specific narrowband fine structure pattern (first recognized during a radio pulsation event) indicates large scale topological changes of the coronal magnetic field.

Key words: radio spectroscopy – radio bursts - coronal shocks - magnetic reconnection

1. Introduction

This paper reviews some recent results of solar decimeter and meter (dm/m) spectral observations. We start our investigation with a list of sites doing solar radio broadband observations. In Section 2 we present the overall context and select two topics: in Section 3 we review results about coronal type II bursts; in Section 4 we demonstrate the significance of combined high resolution spectral and imaging radio observations for a key problem of coronal physics - the fast change of magnetic connectivity during flares (magnetic disconnection and reconnection, e.g. Priest 1982).

Solar radio sources emitting in the meter (300–30 MHz) and decimeter (3 GHz–300 MHz) range are situated in the height range between the chromosphere and about $1.5\,R_\odot$ above the photosphere. Observations in this height range are of basic physical interest: the primary energy release sites of the two most energetic eruptive solar activity phenomena (flares and coronal mass ejections (CMEs, henceforth; see Kahler 1992 for a review) are situated there. Actual space missions (*Yohkoh*, SOHO, TRACE) yield imaging observations of the lowest corona in different spectral ranges and with unprecedented imaging cadence and quality. In the radio range, the Nançay Multifrequency Heliograph (NRH henceforth, see The Radioheliograph Group, 1993) images the sun at 5 frequencies in the range 450–150 MHz achieving a time resolution of up to 0.1 s.

Eruptive energy release disposes of a part of the excess energy into nonthermal particles (e.g., Spicer 1977). The burst emission in the dm/m range is a tracer of otherwise invisible nonthermal electron populations. The bursts are highly variable in frequency, time and intensity. Therefore, continuous frequency coverage is necessary with high time resolution. Image processing of digitally recorded spectra allows one to study the burst emission over the whole dynamic range of the receivers. This is particularly important for the comparative analysis of radio data with observations in other spectral ranges. Table 1 gives an overview of existing full-disk spectrometers. There is no solar dedicated dm/m imaging spectrometer.

2. Overall context and motivation for two subtopics

In contrast with the microwave range (Bastian, this proceedings), the dm/m emission processes are quantitatively unknown (Melrose, this proceedings). Coherent plasma emission is one important radiation mechanism. Plasma instabilities excited by nonthermal electrons yield enhanced high and low frequency plasma wave turbulence. High frequency plasma waves are scattered by low frequency waves, ions or density inhomogeneities interact with oppositely-directed high frequency waves thus leading to radio emission at the fundamental or harmonic of the plasma frequency f_p. Because of $f_p(h) \propto N_e(h)^{1/2}$ [1] we can transform the frequency scale of the frequency-time plane into a height scale using a density model (e.g. Newkirk 1961, Koutchmy 1994, Mann et al. 1998). Then, the radio spectral diagram can be understood as a height-time diagram. It is well known, that the drift rates of bursts driven

1 N_e electron density, h - height in the corona.

Table 1.. **Broadband receivers in the meter and decimeter range**

	Range (MHz)	Time Resolution [s]	Spectral Resolution $2 \cdot \triangle f/f$ [%]
Artemis (Greece)	470 - 110	0.01	0.8
Beijing (China)	3700 - 3400	0.001	-
Bruny Island (Australia)	37 - 3	3	0.1
Culgoora (Australia)	1800 - 18	3	-1.0
Hiraiso (Japan)	2500 - 25	3 - 4	0.2
INPE (Brazil)	2500 - 1000	1 - 0.01	-
IZMIRAN (Russia)	240 - 45	0.1	-
Nançay (France)	75 - 25	0.1	> 0.4
Ondřejov (Czech Republik)	4300 - 800	0.1	0.6
Ooty (India)	80 - 30	-	-
Porto (Portugal)	600 - 200	0.1 or 0.01	> 0.16
Tremsdorf (Germany)	800 - 40	0.1 (0.01)	0.46
USAF (USA, Network)	80(130) - 30	3	-
Zürich (Switzerland)	4000 - 100	< 0.1	0.2

In the right column, we give the density contrast (for effects due to plasma emission) and the part of the coronal scale height which can be resolved by the given spectrometer. The spectrometer of the AI Potsdam at Tremsdorf Observatory (Mann et al. 1992) consists of a system of four sweep spectrographs (as given above), and two multichannel receivers for narrow parts of the interval 800–40 MHz (time res. 0.01 s, spectral resolution 0.08 and 0.28, respectively).

by electron beams (type III bursts) or shock waves (type II bursts) can be used to estimate the exiter's propagation speed along the local coronal density gradient.

As mentioned, solar radio bursts yield the only ground based access to energy release–related nonthermal electron populations in the corona. Radio observations contain information about energy release, electron acceleration and electron transport (Bastian, Benz, and Gary 1998). With respect to the transport the radio signatures can be classified[2] into

1. trapped electron-driven phenomena such as continuum bursts of type IV including some radio continuum fine structures, the flare continua, the type V bursts and the type I noise storm continuum component. The electrons are captured in magnetic traps.

2. electron beam-driven phenomena as bursts of types III, reverse drifting type III (RS henceforth), type U, spike bursts, type I bursts, some radio continuum fine structures. The electron beams propagate essentially once along an open or closed magnetic field line.

3. mixed phenomena as bursts of type II (the backbone emission is probably a continuum-like effect emanating from the shock transition region; the herringbone fine structures are due to beams leaving the shock transition region), type I noise storm chains, and the so-called patchy features.

A continuous spectral coverage of a burst yields the "radio illumination" of the density profile along the propagation path of the nonthermal electrons if the sufficient conditions for plasma radiation are fulfilled. This means radio spectral observations can spectrally resolve density inhomogeneities which are spatially too small for being resolved with an imaging telescope (see the right column of Table I for the resolution of existing spectrographs).

On the other hand, under solar coronal conditions energy release processes and particle acceleration occur in volumes being very small (e.g. Spicer 1977) at least in one dimension. This is true for the diffusion region of reconnecting magnetic field lines (e.g., Priest 1982), but also for the transition region of coronal and interplanetary shock waves (Mann 1995). Spectral radio observations can be a tool to look into such volumes.

2 All terms used in this classification are explained in McLean and Labrum (1985).

There are several pieces of evidence for the importance of the reconnection process for flare energy release and topological changes in the large scale coronal magnetic field (see e.g. Démoulin et al. 1996; Forbes 1996; Tsuneta 1996; Emslie 1996; Kosugi and Somov 1998). *Yohkoh* soft X-ray telescope images (Tsuneta et al. 1991, SXT, henceforth) gave a final confirmation for the fact that cusp–like structures on different spatial scales are an essential structural element for understanding the flare process, the arcade formation, and the acceleration of particles (for example Sakao, Kosugi and Masuda 1998; Aschwanden 1998). Near to the diffusion region of reconnecting field lines, escaping hot gas streams form standing shock waves which are partly detected in hard X–ray emission (the loop top sources firstly described by Masuda et al. 1994, see also Kosugi and Somov 1998). The fast mode bow shocks predicted by Tsuneta (1997) are not yet convincingly associated with a radio signature.

Traveling fast mode coronal shocks driven probably by the flare blast wave, by massive flare ejecta, but possibly also by a CME piston (Gopalswamy et al. 1998; Cliver et al. 1998) are well documented by type II radio bursts. There are some (until now rare) cases of near-to-the-limb events where a flare-related moving bright knot in *Yohkoh* SXT images is seen to move toward the site of the type II radio source (Nitta 1998, personal comm.; Vilmer et al. 1998, poster at CESRA, and this conference).

In recent reviews (e.g. Hudson and Ryan 1995; Bastian, Benz and Gary 1998; Kundu 1998; Shimojo, Shibata and Harvey 1998) attention is devoted to work on type III and type III–like radio bursts and their relation with particle acceleration and jet formation (point 2 of our above given classification). Pick (this proceedings) reviews meter wavelength and coronagraphic observations covering the radio imaging–CMEs–flares aspect as well as the problem of electron propagation and injection in the interplanetary medium thus touching my points 1 and 2. Therefore I focus on my point No. 3 (type II bursts, Section 3).

Sakao, Kosugi and Masuda (1998) statistically derived from hard X-ray data that "loop-with-a-cusp" flares and "emerging-flux-type" (loop-loop interaction) flares produce different electron energy spectra. The authors point out that the relationship between the two pictures "... has so far remained unclear". Emslie (1996) stressed that one crucial observational test for magnetic reconnection is the presentation of further examples of structural rearrangement in relation with magnetic energy release. I have found a case during which a special narrowband radio source definitely appears during a change of magnetic topology. This happens during a flare which consists of a nested combination of the two basic flare geometries discriminated by Sakao, Kosugi and Masuda (1998). Bastian, Benz and Gary (1998) write in their recent review about radio emission of solar flares that the use of "...radio observations as tracers of changing magnetic connectivity ... has not yet been exploited but holds promise ..." Therefore there is some justification to present this matter in the frame of this paper (Section 4).

3. Type II bursts

The most recent review papers about coronal shock waves are Aurass (1997) and Klein and Mann (1997) which give the relation to earlier work. Meanwhile, some new results can be quoted.

Kaiser et al. (1998) have reported a slow drift burst in WIND radio spectra between 14 and 1 MHz. This is probably the first event showing a convincing continuation of a metric type II lane at very low frequencies. The paper does not focus on this point but comes to the conclusion that the low frequency emission argues for two shocks, one driven by the flare blast and one by the CME.

The first X–class flare after the last minimum of activity on 09 July 1996 attracted a lot of attention as the first strong flare event during the SOHO mission. Hudson et al. (1998) presented a long term study of the responsible active region. In a complex event analysis, Dryer et al. (1997) have shown (to the author's knowledge, for the first time) a fully digitally recorded spectrum of a radio burst in the range between 40 MHz and 8 GHz. The spectrum displays the records of three observatories (Bern, Ondrejov, and Potsdam-Tremsdorf). It consists of a comparatively slowly drifting microwave burst (due to the evaporation shock according to Karlický and Odstrčil's 1994 interpretation) which smoothly joins with a complex type II burst. Pick et al. (1998) studied the global relation of metric radio burst components with the later observed SOHO-LASCO coronagrams. Mann et al. (1997) could quantitatively explain SOHO recorded electron data using the Mann and Classen (1995) shock acceleration model. From timing and energy spectrum arguments, the same electron population is shown to be visible in the radio as strong type III-like emission emanating from the type II trace in the spectrum. Klassen et al. (1999) studied the type II burst data more in detail and found that it consists of two different type II burst signatures, where the first appears further away in the corona than the second.

Zlotnik et al. (1998) present evidence that third harmonic type II burst emission is not as rare as believed before the advent of digital radio spectral records. From an analysis of two cases the authors found second / third harmonic temperature ratios of $140 \cdots 1200$ and $4 \cdots 6$, respectively.

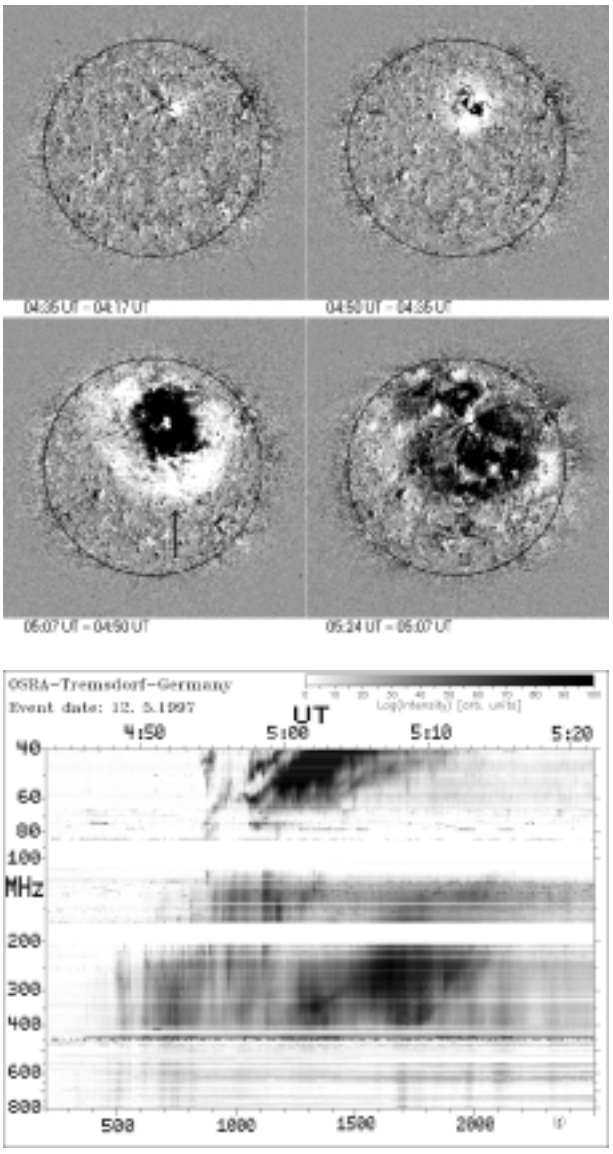

Fig. 1.. The EIT transient wave phenomenon in 195 Å difference frames (courtesy B. Thompson) and the associated radio type II burst spectrum of the event 12 May 1997. 21 cases are shown in a catalogue of events for the year 1997 (Klassen, Thompson et al., 1999).

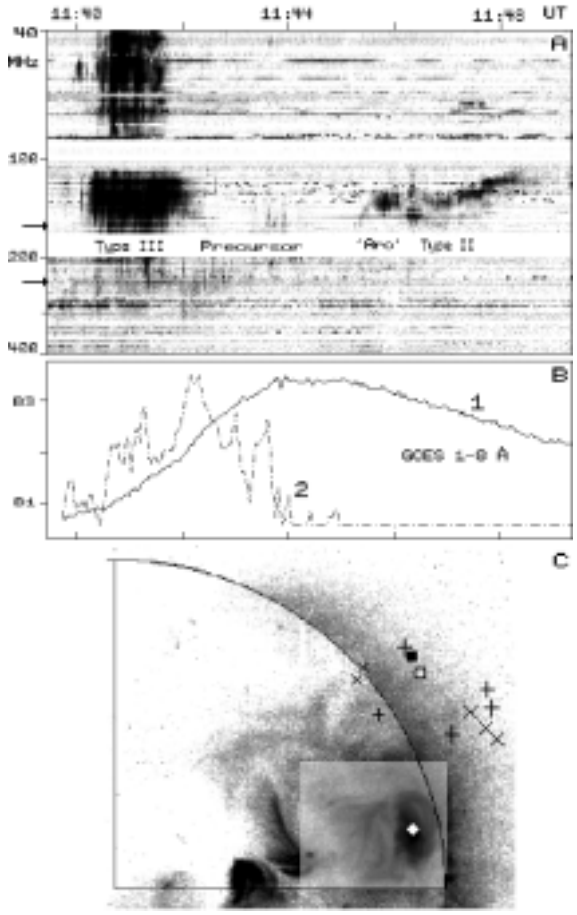

Fig. 2.. Event on 13 July 1994 (from Klassen et al. 1998). (A)–the 40–400 MHz dynamic spectrum after background subtraction. White time-parallel stripes are observational gaps. Arrows point onto NRH frequencies, (B)–GOES soft X-ray flux 1–8 Å (1) and its derivative (2) (units as in SGD- Solar Geophysical Data, B1 = 10^{-4} erg $(\mathrm{cm}^2\,\mathrm{s})^{-1}$, (C)–burst positions superposed upon the *Yohkoh* SXT image (12:33 UT): $\diamond$ – H_α flare, $\times$ ($\times$) – the ascending (descending) branch of the group of type III, J and U bursts at 164 MHz, $+$ (+) – the ascending (descending) branch of *type II precursor* at 164 and 236 MHz, square with dot – *arc*, black square – type II burst. North is top; west is right.

Klein et al. (1997) compared the type II burst source site of an occulted flare with SOHO-LASCO coronagrams. The shock wave seems to be faster than the coronagraphic CME signature. Aurass, Hofmann and Urbarz (1998) compared the type II source sites of an azimuthally moving shock signature with the background magnetic field structure derived by field extrapolation. They found observational evidence for Mann and Classen's (1995) prediction that the shock accelerates electrons during quasi-perpendicular **and** quasi-parallel propagation to the local magnetic field. Klassen, Thompson et al. (1999) assembled a catalogue of type II burst radio spectra and associated SOHO-EIT coronal transient wave phenomena (Thompson et al. 1998a, b) for the year 1997. Figure 1. shows the 12 May 1997 event. Generally, each coronal EIT transient wave seems to be associated with a type II burst (but not vice versa). The transient wave speed is three- to fivefold smaller than the speed derived from the type II drift rate. Until now, due to the still comparatively low image sequence of SOHO-EIT it is not yet possible to make statements about the time correlation between the onset of both phenomena. This points us to the problem of the identification of the type II driving disturbance from earlier (higher frequency) signatures of this disturbance in the radio spectrogram. Klassen et al. (1998) combined spectral and imaging observations of type II radio events with *Yohkoh* SXT data and with extrapolated magnetic field maps. Two new radio features were identified (see Figure 2.):

1. *Type II precursors* are groups of fast drift bursts with a restricted bandwidth observed in coronal loops from the impulsive flare phase until the onset of the type II emission. These groups are found in the spectrum near

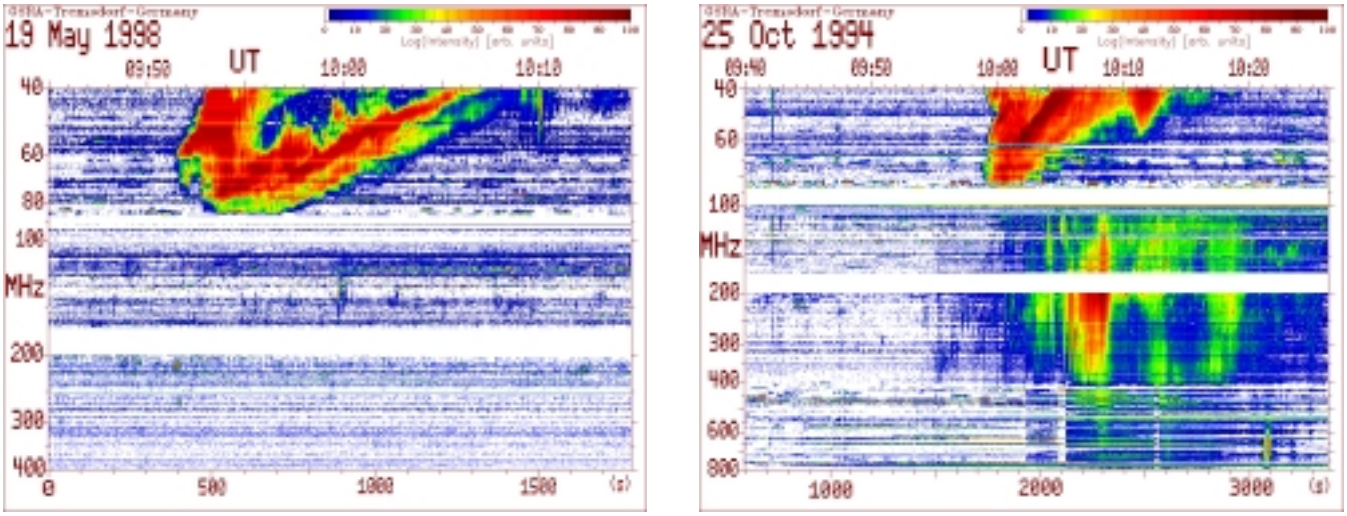

Fig. 3.. Left (a): The type II burst of 19 May 1998. Before the type II burst, no precursor signatures can be identified. There is persistent noise storm activity during the whole observing day, during the type II some type III bursts appear at higher frequencies. Between 90–100 as well as 170–200 MHz there are data gaps due to strong interference. Right (b): The 25 October 1994 flare in AR 7792, the 40–800 MHz radio burst spectrum. In contrast with the event shown in the left the type II precursor activity is clearly visible. In both cases an undisturbed pre-event spectrum was subtracted.

to the backward extrapolated type II lanes. The sources are located **between** the sites of H_α emission and of the type II emission.

2. *Arcs* are a series of narrowband bursts, ≤ 1 min duration, occurring at frequencies between the split bands of the type II lanes just before type II emission. Arcs have a type U–shaped spectral envelope, fundamental-harmonic structure like the subsequent type II burst, but no band splitting. The source is located near the summits of the loops where the precursor occurred, and close to the site of type II emission.

These results close the observational gap between impulsive energy release signatures in the lowest layers of the solar atmosphere and the appearance of the shock-excited radio trace in comparatively large coronal heights (0.2 – 0.5 $R_\odot$). The coronal type II burst is related to a plasma jet or a blast wave that originates in closed active region loops, and is (in radio emission) first recognized during the early impulsive phase due to the precursor. After reaching the summit of the local closed loop structures the disturbance excites the arc feature introducing shock wave formation above the loop's summit. The shock propagates into overlying field regions becoming visible as the well-known type II emission.

For flare-related type II bursts this result confirms Aurass (1997) and Gopalswamy et al.(1998) that the most probable drivers of coronal shock waves are the flare blast wave or a flare–related piston. This does not principally exclude the possibility of prominence- or CME driven coronal shock waves. Spectral observations will not show precursor bursts in case of prominence eruption–driven type II bursts. This is true, for instance, for the burst shown in Figure 3.a which was excited during a prominence eruption (Gopalswamy, personal communication).

4. Evidence of changing magnetic connectivity during a radio pulsation event

The justification of our interest in discussing examples of changing magnetic connectivity in the corona was derived in Section 2. The 09:50 UT flare in AR 7792 (October 25, 1994) has been discussed already by Manoharan et al. (1996a, b) and Aurass et al. (1996, paper I henceforth).

4.1. The spectrum

The radio event Figure 3.b begins with a type III burst (09:42 UT, 300–40 MHz). At low frequencies, the spectrum is dominated by a bandsplit type II burst starting at about 100 MHz and drifting toward lower frequencies (09:59–

10:14). Before the type II burst (past 09:52) there appear some faint features in the range 400–140 MHz which are already accompanied by impulsive hard X-ray emission. This is mainly type II precursor emission (see Section 3). At frequencies above 100 MHz a continuum with spectral fine structures (pulsations, later zebra pattern, e.g. Kuijpers 1980) appears simultaneously with the low frequency type II burst. The continuum forms three enhancements (the main effect until 10:09; further 10:11–10:15 and 10:17–10:20). The gradual decay of the event after 10:20 UT is interrupted by a brief dm pulse observed at 10:21 UT between 600 and 800 MHz. This pulse is rich in fiber burst fine structures.

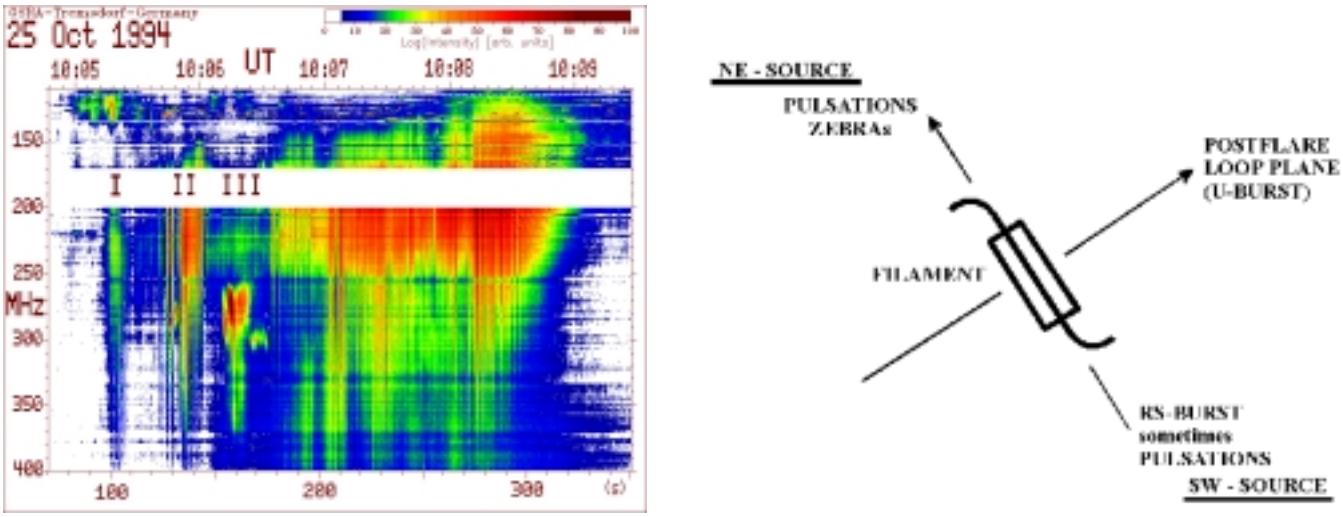

Fig. 4.. Left (a): The modulated 1.5 s broadband pulsations of the metric continuum between 10:05 and 10:09 UT. Especially, note the narrowband pattern appearing at about 280 MHz on 10:05:48 and 10:06:12 UT and see the enlargements given in Figure 6.. I, II, III denote three flux enhancements. Right (b): Scheme of radio burst source sites as observed by the NRH at 327 MHz (after paper I).

Figure 4.a gives a detailed radio spectrum of the broadband pulsations starting at about 10:05 and reforming at the low frequency side to a zebra pattern past 10:08 UT. The pulsations are not continuously excited but a long period (about 35 s) is superposed to the basic 1.5 s periodicity. The pulsations grow in three morphologically resemblant pulse trains to a maximum achieved in a fourth enhancement at about 10:07:10 UT. Within these pulse trains there appears a remarkable narrowband feature (NBF, henceforth). It can be identified first in pulse train II, strongest and dominating in pulse train III. The proper pulsation diminishes in this third pulse.

The NBF consists of a two-patch pattern detailed in Figure 6.b. The bandwidth of a single patch is about 3.5 %, the first appearing at a 3 % higher frequency than the second (more intense) one. The time delay between the two pulses is 1.2 s. The stronger effect (pulse III) shows some more details than the fainter one, among others a third patch, a 7 s duration lane at the high frequency edge, and–most important–a RS burst escaping from the major narrowband brightening and decaying at about 370 MHz. This means the drift burst–exciting electron beam stops radiating at densities about 1.7 times higher than in the acceleration site which we associate with the source site of the narrowband brightenings.

4.2. Soft X-ray images of AR 7792

This radio flare is due to nonthermal electrons energized during the transition of a preflare inverted S–shaped loop system into a relaxed three–loop postflare pattern (see also Sakurai 1993 studying a comparable event). We use in the following the term *sheared quadrupolar configuration* in the sense of Uchida (1980), Uchida et al. (1996) and Uchida, this conference.

Figure 5.a gives superposed *Yohkoh* partial frame images of the active region immediately before and after the flare. If one measures the X-ray flux evolution of three SXT image pixel groups A, B, and C defined by the postflare loop pattern one obtains Figure 5.b. It shows that the three postflare loop configurations are formed sequentially in time. Note that there are also three radio continuum enhancements between 10:07 and 10:20 UT (comp. Figures 5.b

and 3.b). This may indicate that the three postflare loops are activated step by step in the order A - B - C [3]. Each postflare loop activation is accompanied by a certain amount of thermal and nonthermal energy release. Thereby, the formation of loop A is most efficient.

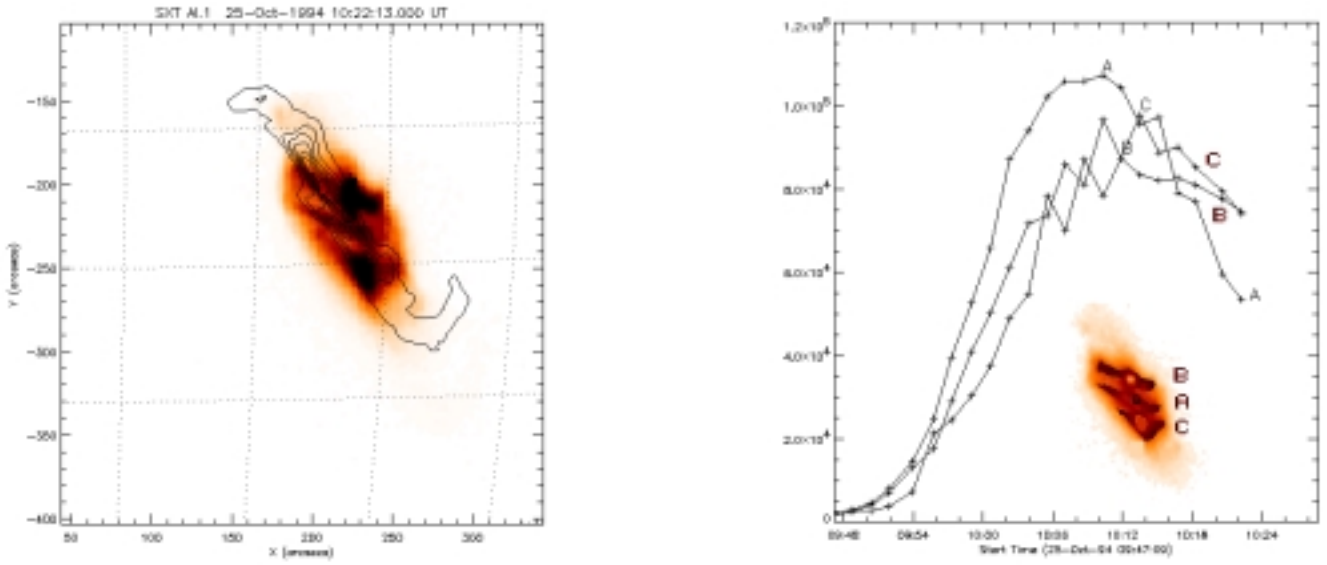

Fig. 5.. Left (a): *Yohkoh* SXT pre- and postflare partial frame images of AR 7792. Superposed are the images of 09:47 (isolines) and 10:22 UT (color coded). Right (b): Soft X-ray brightness of the postflare loop - associated pixels during the flare in arb. units. The insert (dark brown areas) denotes the postflare loop pixel-sets B–A–C from top to bottom.

4.3. The radio source site distribution

Probably due to the isolated appearance of AR 7792 on the disc the source sites of the radio flare and those belonging to the postflare evolution are widely distributed on the disc and can be unusually clearly discriminated from each other. A global source site analysis is presented using NRH data (orthogonal scans at five frequencies) in paper I, and by Aurass and Klein (1997). The situation is sketched in Figure 4.b. A background flare continuum and the type II precursor bursts are situated above the active region. The broadband pulsations are formed at least at 327 MHz by two widely separated subsources - one northeast, the other southwest of the active region. A whole sequence of type U bursts - the first during the flare (10:07:48 UT, see also Figure 7.), the others up to five hours after the impulsive phase - describe with the source sites of their rising and descending branches a plane perpendicular to the line which interconnects the fine structure sources (for details see Aurass and Klein 1997). In the given event it is impossible[4] to image the NBFs in pulses II and III of the broadband pulsations. But fortunately, the RS burst appearing during pulse III can be localized at least at 327 MHz (far from the electron injection site). At this frequency its source is situated at the southwestern fine structure site.

4.4. The source-site interplay during fine structure evolution

Figure 6. gives the enlarged NBF spectra, and the radio flux curves at 327 MHz in the time interval 10:05 - 10:08 UT obtained by integrating over three source areas using the NRH data (courtesy K.- L. Klein, Paris-Meudon Observatory). As evident from the flux curves, the 327 MHz fine structure source is localized at the NE site during pulsation trains I and II (see Figure 4.a for No.s I–III). During pulse III, the RS burst source is situated above the active region (AR) and at the SW site, only[5]. After pulse III, the pulsations result from more or less correlated flux enhancements **in both** the NE and the SW source. A detailed pulse-by-pulse analysis is in preparation.

3 Here, the notation of the three loops is changed in contrast with paper I.
4 due to the rough frequency grid of the NRH
5 The small negative flux values during pulse III at the NE site are an artifact.

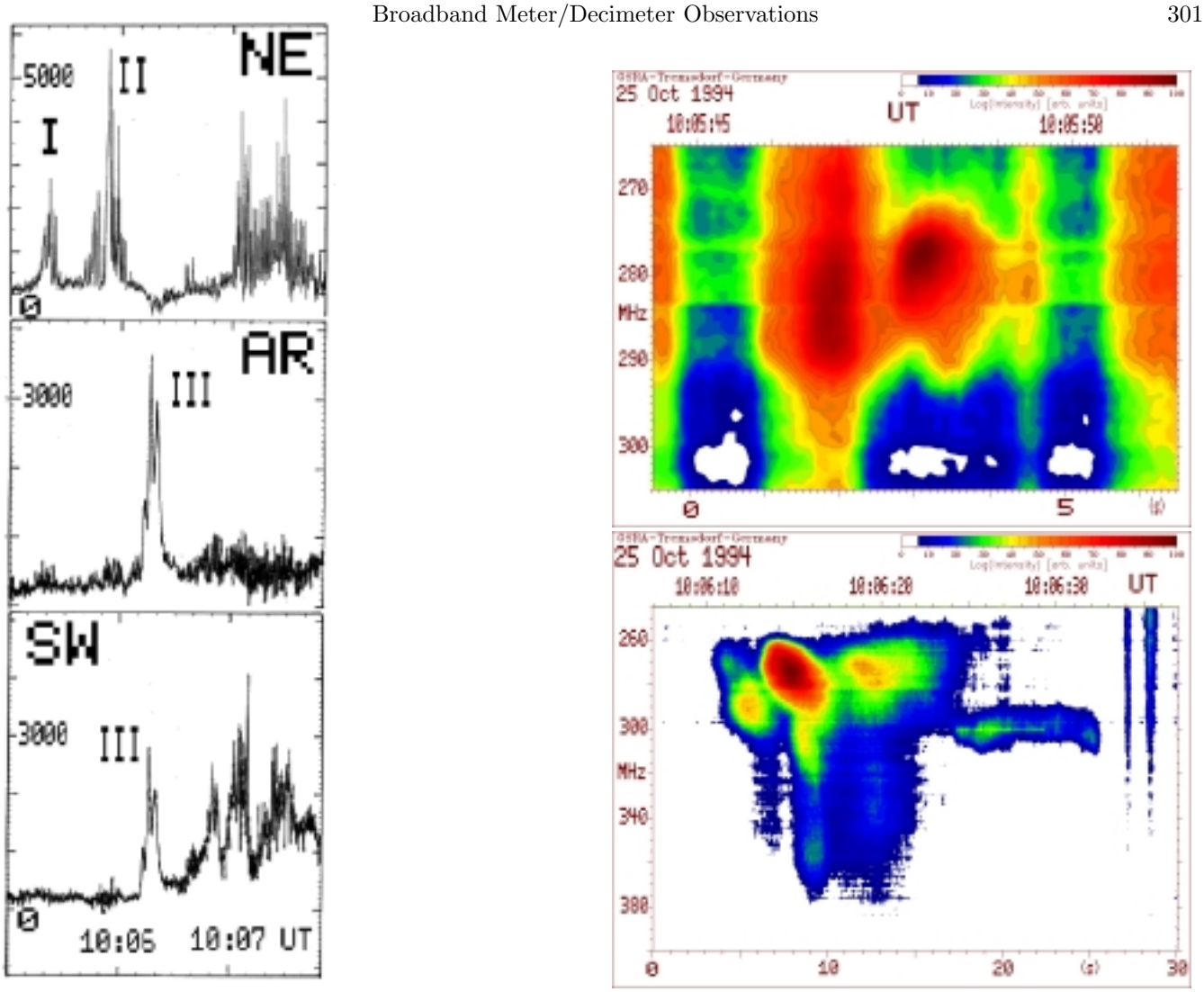

Fig. 6.. Left part (a): flux curves at 327 MHz (NRH, courtesy K.-L. Klein) for three different regions on the disc (compare also Figure 4.b). Right part (b): the narrowband patterns of Figure 4.a enlarged (top–patch pattern during pulse II, bottom–the same during pulse III). The pattern during pulse III signifies the formation of a new magnetic connection between the electron acceleration site in AR and the SW source. During pulses I and II, the source of nonthermal electrons is still connected with the NE source site, only.

Summarizing we notice that pulse III acts like a switch-on for the simultaneous pulsating emission from the NE and the SW sources.

Figure 7.b gives the spectrum of the type U burst (turnover frequency 400 MHz) appearing at the high frequency edge of the broadband pulsations at 10:07:48 UT. The 435 MHz source sites of the rising and the descending branch source of this burst are shown in Aurass and Klein (1997) to be situated in the plane of the postflare loops above the active region with the rising branch source east of the photospheric magnetic neutral line (MNL), the descending branch source west of the MNL. Figure 7.a outlines NRH 327 MHz flux curves, but only of the NE and the SW source regions. Remarkably, we find that the 327 MHz fine structure emission at the SW source decays after the type U burst. We notice that the U burst signals an switch-off of the correlated pulsating emission between the widely separated NE and SW sources. Later, the fine structure source is localized at the NE source site as before during pulses I and II (compare Figure 6.a).

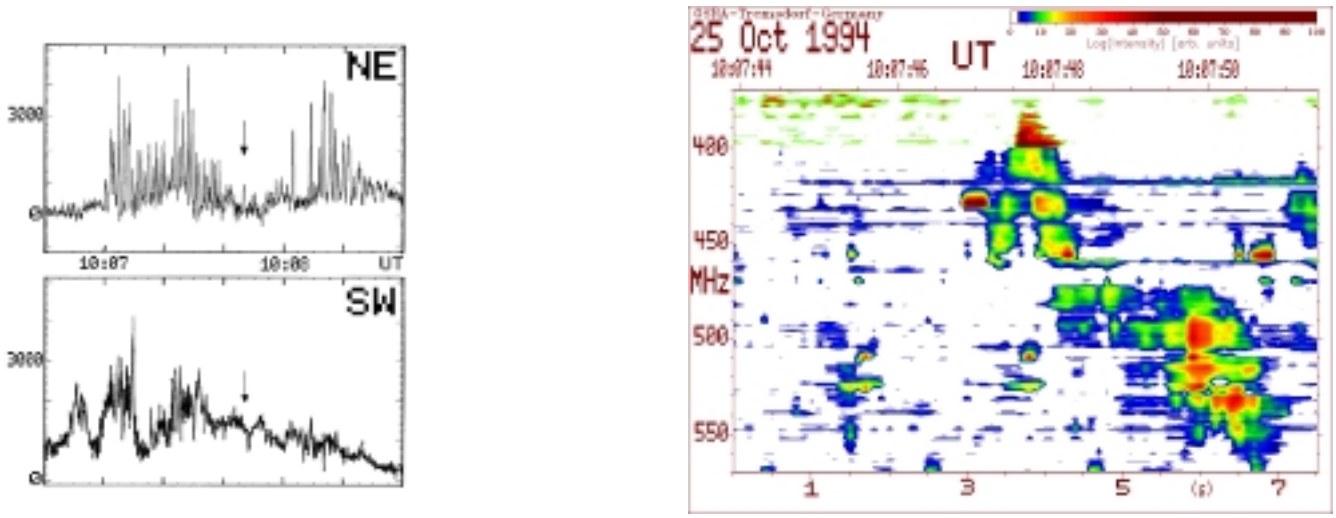

Fig. 7.. Left part (a): 327 MHz NRH flux curves for regions NE and SW 10:06:40–10:08:40 UT (courtesy K.- L. Klein). The arrow is the time of the 450–400 MHz U burst. Right part (b): the type U burst at 10:07:48 UT. This burst marks the disconnection between the electron acceleration site above the AR and the SW source, as well as the passage of a beam along the newly formed postflare loop A.

4.5. Interpretation

The main radio features of the 25 October 1994 event inform us about the stepwise "activation" of different pre- and postflare magnetic structures. In Figure 8., we have schematically sketched a probable field line pattern and the acting acceleration sites. This scheme is different from the scenario proposed by Manoharan et al. (1996b). The quadrupolar sheared preflare loop system indicated by S-shaped loops (Figure 5.) is replaced by three low-lying soft X–ray post-flare loops. The electrons exciting radio pulsations propagate along field lines of the northern inverted S-shaped preflare pattern toward the NE source site. The post-flare loop A is first activated. This process determines the radio emission between 10:05 and 10:10 UT.

The spatial arrangement of the pulsating radio sources around the active region and their flux dynamics reveal that the necessary source of nonthermal electrons for the pulsating emission must be directly in the active region. A detailed investigation of H_α data (B. Vršnak and V. Rudžjak, personal comm.) and the comparison with the extrapolated magnetic field lines above the active region (A. Hofmann, personal comm.) reveal that this site is near to a single big sunspot west of the MNL and connected with a small but quickly evolving island of parasitic emerging flux in its surroundings. The configuration corresponds with Hanaoka's (1996, 1998) sketch of a "three–legged structure", and *Yohkoh* SXT images reveal also jet activity at this site hours before the flare. It is nested as an emerging–flux–type configuration within and below a superposed sheared two–ribbon (loop–with–a–cusp in terms of Sakao et al. 1998) configuration.

According to the radio data presented the three–legged magnetic structure ejects streams of nonthermal electrons with a period of 1.5 s. These electrons lead to broadband pulsations mainly in the NE radio source. In the given case, the periodicity is caused by quasiperiodic electron injection (see e.g. Kuijpers et al. 1981) and not by the dynamics of trapped particles (Zaitsev and Stepanov 1975).

Only during the 1.5 min between the brightest narrowband emission pattern at about 280 MHz (pulse III, see Figures 4. and 6.) and the U burst between 450 and 400 MHz (Figure 7.) , the accelerated electrons are injected in the NE and the SW source. This means a new magnetic connection was formed branching near to the narrowband source site in the active region and remained stable for 1.5 minutes. Thereafter, the particle stream path switches back into nearly the initial state. Meanwhile, loop A was activated and is passed by an electron beam injected from a new acceleration site east of the MNL in the active region. Further U bursts follow in the later postflare stage (see Aurass and Klein 1997).

The presented facts lead to the claim that we have seen magnetic reconnection between field lines belonging to a comparatively small scale three–legged–loop configuration and the overlying large scale sheared quadrupolar

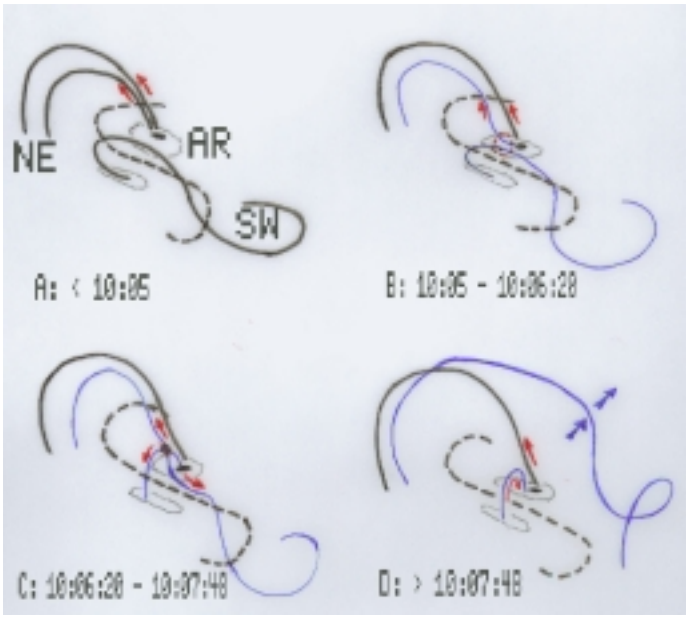

Fig. 8.. A perspective scheme of "activated" field lines respecting only postflare loop A of Figure 5.. The stippled curve is the magnetic neutral line in the photosphere. Red arrows are streams of nonthermal electrons. The blue magnetic field lines are subject of a dynamic evolution. The black dot in AR denotes the dominating leading sunspot. A: A pulsating source is formed between AR and NE due to a low lying "three–legged–loop" structure (Hanaoka 1998). B: The two blue loops approach each other. In the contact region (red stippled circle) the narrowband radio sources of pulses II and III are situated. The RS burst source during pulse III is seen at SW. C: Pulsating sources at NE and SW commonly contribute to broadband pulsations. Nonthermal electrons are accelerated in the AR and escape toward NE **and** toward SW, simultaneously. D: One field line AR–NE and one field line AR–SW (former belonging to the S–shaped preflare SX–loops) merge to form a large rising loop structure. Their AR–roots reconnect to form the postflare loop which is passed by an U burst–exciting beam (see Figure 7.).

configuration. We have evidence for dynamically changing magnetic paths seen by electrons accelerated in the innermost part of the active region atmosphere. Further, we have found the decisive role of a spatially small volume: the branching of electron paths after the NBF at 280 MHz. We believe that the NBF source encloses the diffusion region. From the radio emission frequency follows a density of 2.4 (or 9.6^6) $\cdot\, 10^8\,\mathrm{cm}^{-3}$. From the type U burst's turning frequency follows that the density at the top of activated postflare loops is about half of those in the NBF source region.

Altogether, three independently existing and spatially separated electron acceleration sites form the sources of dynamically changing radio continuum fine structures:

1. the three–legged–loop structure near a big sunspot at the southern footpoint range of NE–wards leading loops (northern part of the preflare images, Figure 5.) responsible for pulsed electron streams detected as broadband pulsations and later zebra pattern,

2. the acceleration site between the deformed NE– and SW–branches of the inverted S pattern exciting the NBFs near 280 MHz in pulses II and III, see Figures 4. and 6.. This is the interaction site between the three–legged–loop and the overlying sheared quadrupolar configuration in an estimated height of about $0.16\,\mathrm{R}_\odot$[7].

3. an acceleration site acting near the eastern footpoint of postflare loop A exciting the U burst shown in Figure 7..

Note that we omit here a discussion of the postflare loops B and C. An extended discussion of the magnetic field topology during the October 25, 1994 event is in preparation.

---

6 if the narrowband source is due to fundamental mode plasma emission
7 applying a fourfold Newkirk density model

5. Conclusion

The advent of fast digital data processing techniques and the regular access to space based imaging information in X-rays and EUV as well as coronagraphic observations of the sun down to 0.1 $R_\odot$ above the photosphere provide a new look on the decimetric and metric radio observations. Broadband radio data are a unique source yielding information about impulsive nonthermal energy release in otherwise inaccessible small-scale magnetoplasma structures.

I have tried to demonstrate the use of decimetric and metric radio observations for approaching answers about essential problems in solar flare physics. We are now able to trace continuously the flare released energy pulse which eventually forms the type II burst exciting coronal shock wave from the chromosphere up to the lower corona. We begin to understand some radio spectral features (the type II precursors) whose importance has until now not been appreciated. We know a typical spectral feature (the arc) which accompanies the escape of the type II driver from closed magnetic loop structures.

Further, I have demonstrated how nonthermal electrons mark changing magnetic connectivities during a broadband radio pulsation event. Thereby, radio spectral data yield otherwise unavailable experimental facts about time scales, densities and connectivities during magnetic reconnection and postflare loop formation under coronal circumstances. To the author's knowledge, we attempt here for the first time a detailed association between a dynamically changing fine structure evolution (broad band pulsations and phase–related narrow band patches) and the changing paths of nonthermal electrons in the related complex magnetic field pattern in the lower corona.

Looking forward to the HESSI mission, and to a detailed analysis of the enormous amount of *Yohkoh*, SOHO, and TRACE data, a newly growing importance of solar radio observations is expected for a better understanding of plasma processes in solar and stellar atmospheres.

Acknowledgements

Thanks are due to the organizers of the conference, especially to Drs. Shibasaki and Bastian. Further, I am grateful to the Japan Society for the Promotion of Science and the Deutscher Akademischer Austauschdienst for paying for my visits at Japan. I acknowledge the discussions with Drs. Uchida and Kosugi, and the access to *Yohkoh* data at MSSL and ISAS. The present work would have been impossible without the cooperation with Drs. Klein, Vršnak, Ruždjak and Hofmann, as well as without the support of my colleagues at AI Potsdam, Solar Radio Astronomy Group.

References

Aschwanden, M. 1998, in Watanabe et al., p. 285
Aurass, H., Klein, K.–L., Martens, P.C.H. 1996 (paper I), in Bentley and Mariska (1996), p. 194
Aurass, H. 1997, in G. Trottet (ed.) *Coronal Physics from Radio and Space Observations*, Lecture Notes in Physics Vol. 483, Springer, Berlin–Heidelberg–New York, p. 135
Aurass, H. and Klein, K.-L. 1997, A&A Suppl. 123, 279
Bastian, T.S., Benz, A.O., Gary, D.E. 1998, Ann. Rev. Astron. Astrophys. 36, 131
Bentley, R.D., Mariska, J.T. (eds.) 1996, *Magnetic Reconnection in the Solar Atmosphere*, PASP Vol. 111
Cliver, E., Webb, D.F., Howard, R.A. 1998, Solar Phys., submitted
Démoulin, P., Henoux, J.C., Priest, E.R., Mandrini, C.H. 1996, A& A 308, 643
Dryer, M., Andrews, M.D., Aurass, H., and 21 coauthors 1998, Solar Phys. 181, 159
Emslie, A.G. 1996, in Bentley and Mariska, p. 419
Forbes, T.G. 1996, in Bentley and Mariska, p. 259
Gopalswamy, N., Kaiser, M.R., Lepping, R.P., and 6 coauthors 1998, JGR 103, 307
Hanaoka, Y. 1996, in Bentley and Mariska, p. 200
Hanaoka, Y. 1998, in Watanabe et al., p. 197
Hudson, H.S., Labonte, B.J., Sterling, A.C., Watanabe, T. 1998, in Watanabe et al., p. 237
Hudson, H.S., Ryan, J. 1995, Ann. Rev. Astron. Astrophys. 33, 239
Kahler, S.W. 1992, Ann. Rev. Astron. Astrophys. 30, 113
Kaiser, M.L., Reiner, M.J., Gopalswamy, N., Howard, R.A., St.Cyr, O.C., Thompson, B.J., Bougeret, J.L. 1998, Geophys. Res. Lett. 25, 14, 2501
Karlický, M., Odstrčil, D. 1994, Sol. Phys. 155, 71
Klassen, A., Aurass, H., Klein, K.- L., Hofmann, A., Mann, G. 1998, A&A in press
Klassen, A., Karlický, M., Aurass, H., Jirička, K. 1999, Sol. Phys., accepted
Klassen, A., Thompson, B.J., Aurass, H., Mann, G. 1999, A&A Lett., submitted

Klein, K.-L., Klassen, A., Aurass, H., LASCO Consortium 1997 in *Proc. of the 5th SOHO Workshop*, ESA–SP404, 461
Klein, K.-L., Mann, G. 1997, in G. Trottet (ed.) *Coronal Physics from Radio and Space Observations*, Lecture Notes in Physics Vol. 483, Springer, Berlin–Heidelberg–New York, p. 161
Kosugi, T., Somov, B.V. 1998, in Watanabe et al., p. 297
Koutchmy, S. 1994, Adv. Space Res. 14, 4, 29
Kuijpers, J. 1980, in M.R. Kundu and T.E. Gergely (eds.) *Radio Physics of the Sun*, Proc. IAU Symp. No. 86, Reidel, Dordrecht, p. 341
Kuijpers, J., van der Post, P., Slottje, C. 1981, A & A 103, 331
Kundu, M.R. 1998, in *Solar Jets and Coronal Plumes*, ESA–SP421, p. 179
Mann, G., Aurass, H., Voigt, W., Paschke, J.: 1992, in *Coronal Streamers, Coronal Loops and Coronal and Solar Wind Composition*, ESA–SP348, p. 129
Mann, G. 1995, in A.O. Benz and A. Krüger, Lecture Notes in Physics Vol. 444, Springer, Berlin–Heidelberg–New York, p. 183
Mann, G., Jansen, F., MacDowall, R.J. 1998, *Kleinheubacher Berichte*[8] 41, p. 267
Manoharan, P.K., van Driel-Gesztelyi, L., Pick, M., Démoulin, P. 1996a, PASP 111, p. 398
Manoharan, P.K., van Driel-Gesztelyi, L., Pick, M., Démoulin, P. 1996b, ApJ 468, L73
Masuda, S., Kosugi, T., Hara, H., Tsuneta, S., Ogawara, Y. 1994, Nature 371, 495
McLean, D.J., Labrum, N.R. (eds) 1985, *Solar Radiophysics*, Cambridge Univ. Press, Cambridge, UK
Newkirk, G.A. 1961, ApJ 133, 983
Pick, M., Maia, D., Kerdraon, A., and 10 coauthors 1998, Sol. Phys. 181, 455
Priest, E.R. 1982, *Solar Magnetohydrodynamics*, Reidel, Dordrecht–Boston–Lancaster
Sakao, T., Kosugi, T., Masuda, S. 1998, in Watanabe et al. (1998), p. 273
Sakurai, T. 1993, Adv.Space Res. 13, 9, 109
Shimojo, M., Shibata, K., Harvey, K.L. 1998, Sol. Phys. 178, 379
Spicer, D.S. 1977, Solar Phys. 53, 305
The Radioheliograph Group 1993, Adv. Space Res. 13, 9, 411
Thompson, B.J., Plunkett, S.P., Gurman, J.B., Newmark, J.S., St.Cyr, O.C., Michels, D.J. 1998, Geophys. Res. Lett. 25, 14, 2465.
Thompson, B.J., et al. 1998, ApJ Lett.
Tsuneta, S. et al. 1991, Sol. Phys. 136, 37
Tsuneta, S. 1996, in Bentley and Mariska, p. 409
Tsuneta, S. 1997, ApJ 483, 507
Uchida, Y. 1980, in *Skylab Workshop, Solar Flares*, ed. P.A. Sturrock, Univ. Colorado Press, 67 and 110
Uchida, Y., Fujisaki, K., Morita, S., Hirose, S. 1996, p. 347
Watanabe, T., Kosugi, T., Sterling, A.C. (eds.) 1998, *Observational Plasma Astrophysics: Five Years of Yohkoh and Beyond*, Astrophys. and Space Science Lib. Vol. 229, Kluwer Dordrecht–Boston–London
Zlotnik, E.Ya., Klassen, A., Klein, K.-L., Aurass, H., Mann, G. 1998, A & A 331, 1087
Zaitsev, V.V., Stepanov, A.V. 1975, A & A 45, 135

8 and A&A in press